

Non-Markovian dynamics of double quantum dot charge qubits due to acoustic phonons

M. Thorwart¹, J. Eckel¹, and E. R. Mucciolo^{2,3}

¹*Institut für Theoretische Physik, Heinrich-Heine-Universität Düsseldorf, D-40225 Düsseldorf, Germany*

²*Department of Physics, University of Central Florida, Box 162385, Orlando, FL 32816-2385, USA*

³*Departamento de Física, Pontifícia Universidade Católica do Rio de Janeiro, C.P. 37801, 22452-970 Rio de Janeiro, Brazil*

(Dated: October 24, 2018)

We investigate the dynamics of a double quantum dot charge qubit which is coupled to piezoelectric acoustic phonons, appropriate for GaAs heterostructures. At low temperatures, the phonon bath induces a non-Markovian dynamical behavior of the oscillations between the two charge states of the double quantum dot. Upon applying the numerically exact quasiadiabatic propagator path-integral scheme, the reduced density matrix of the charge qubit is calculated, thereby avoiding the Born-Markov approximation. This allows a systematic study of the dependence of the Q -factor on the lattice temperature, on the size of the quantum dots, as well as on the interdot coupling. We calculate the Q -factor for a recently realized experimental setup and find that it is two orders of magnitudes larger than the measured value, indicating that the decoherence due to phonons is a subordinate mechanism.

PACS numbers: 03.67.Lx, 03.65.Yz, 73.63.Kv, 63.20.Kr

I. INTRODUCTION

Various candidates for realizing building blocks of quantum information processors with nanoscale solid state structures have been proposed and also partially realized in ground-breaking experiments. An important class of proposals consists of using the charge degree of freedom in semiconducting double quantum dots (DQDs)^{1,2} to realize a quantum mechanical two-state system or quantum bit (qubit).^{3,4,5,6} Thereby, the logical states $|0\rangle$ and $|1\rangle$ are given by the low-energy charge states of the DQD with one excess electron either on the left or the right dot. The transition between these states occurs via tunneling between the two dots. A significant advantage of the charge qubit is its direct controllability via external voltage sources. In recent experiments, the coherent manipulation of charge states of DQDs has been achieved.^{7,8,9} Thereby, the control over the bias and the gate voltages permits to reliably tune the DQD in the Coulomb blockade regime to the required transition line $(1, 0) \leftrightarrow (0, 1)$. The large charging energies suppress leakage to energetically higher lying many-electron states.

A central impediment for coherent quantum information processes is decoherence and dissipation, see Ref. 10 for a particular example. Since charge qubits are rather easily addressable from outside, they are, in turn, also rather fragile for various decoherence mechanisms from the environment. In order to achieve a thorough understanding of the role of the various decoherence mechanisms, one has to rely on realistic and precise model calculations which allow to sort out the different contributions. Among them, decoherence due to acoustic phonons is one possible candidate. This mechanism has been studied previously upon using approaches relying on the Born-Markov approximation.^{2,6,11,12} The decoherence rates obtained in these studies were one or two orders of magnitude smaller than those determined experimentally for GaAs DQDs.^{7,8} However, no exact treatment was available to validate the Born-Markov approximation in the DQD context. This is particularly interesting in view of realistic DQD designs since geometrical form factors tailor a rather peculiar

spectral density $J(\omega)$ of the phonon environment. For piezoelectric phonons, it has a high-frequency tail decaying only algebraically with¹¹ $J(\omega) \propto \omega^{-1}$ while it is superohmic at low frequencies with $J(\omega) \propto \omega^3$, with a crossover at frequencies in the regime of the tunneling amplitude of the DQD. As it has also been pointed out in Ref. 11, the use of the Born-Markov approximation is appropriate only at small tunneling amplitudes. However, it is expected to become increasingly unreliable at DQD with larger interdot tunneling amplitudes. The motivation to find exact reference solutions for this problems also stems from the fact that the Born-Markov approximation has led to the conclusion that other mechanisms of decoherence, as for instance, background charge fluctuations and electromagnetic noise from voltage fluctuations, would be the dominating source of decoherence while phonon decoherence should be a negligible contribution. In view of further design optimization for real devices, exact results are clearly desirable.

In this paper, we study phonon decoherence using the same model as in Ref. 11 as a basis for the numerically exact iterative quasiadiabatic propagator path integral (QUAPI) scheme.^{13,14,15} In particular, we avoid the Born-Markov approximation which turns out to be problematic at larger tunneling amplitudes Δ of the DQD. The decaying oscillations of DQD charge states allows us to extract the quality (or Q -) factor. We find that Q decreases with increasing tunneling amplitudes Δ for small Δ . In fact, the solution in this regime is accurately described by the weak-coupling result for a superohmic environment.¹⁶ At large Δ , the Q -factor increases with increasing Δ and the non-Markovian corrections become noticeable changing even the order of magnitude of Q . In between these two regimes, a crossover occurs which is related to the geometry of the DQD, see below. In particular, our numerical precise method allows to obtain results for the DQD device recently realized in experiments.^{7,8} We find that the calculated value lies approximately two orders of magnitude above the experimentally measured value. Indeed, this suggests that the phonon decoherence mechanism is subordinate and other mechanisms dominate decoherence in DQD

charge states which have been realized until now. In comparison to the results from the Born-Markov approximation, we find that the exact Q -factor is in general larger, indicating that the former overestimates phonon decoherence.

II. MODEL FOR CHARGE QUBIT AND PHONON BATH

In order to solely investigate the role of the phonons in the decoherence processes, we start with the simplifying assumption that the DQD is isolated from the leads. The total Hamiltonian is given by^{6,16}

$$H = H_S + H_B + H_{SB}. \quad (1)$$

Here, H_S is the Hamiltonian of the DQD which is modeled in the basis of the two localized charge states $|0\rangle \equiv |L\rangle \equiv (1, 0)$ and $|1\rangle \equiv |R\rangle \equiv (0, 1)$ as a symmetric two-level-system in pseudo-spin notation (σ_i are the Pauli matrices) as

$$H_S = \hbar\Delta\sigma_x. \quad (2)$$

In this simple model, we have assumed that the external gate voltage is tuned such that the two charge states are energetically nearly degenerate and that the excess electron can tunnel between the two dots with the tunneling amplitude Δ . A possible energy bias between the two states could easily be included in the model but is not considered in this work.

The Hamiltonian for the phonon bath is, as usual, given by

$$H_B = \hbar \sum_{\mathbf{q}} \omega_{\mathbf{q}} b_{\mathbf{q}}^{\dagger} b_{\mathbf{q}}, \quad (3)$$

with the phonon dispersion relation $\omega_{\mathbf{q}}$.

The interaction part of the Hamiltonian is determined by the electron-phonon interaction and reads^{2,6,11,17}

$$H_{SB} = \hbar \sum_{\mathbf{q}} (\alpha_{\mathbf{q}}^L N_L + \alpha_{\mathbf{q}}^R N_R) (b_{\mathbf{q}}^{\dagger} + b_{-\mathbf{q}}). \quad (4)$$

Here, N_{ξ} is the number of the excess electrons on the left/right ($\xi = L/R$) dot and $\alpha_{\mathbf{q}}^{\xi} = \lambda_{\mathbf{q}} e^{-i\mathbf{q}\cdot\mathbf{R}_{\xi}} F_{\xi}(\mathbf{q})$ where $\mathbf{R}_L = 0$ and $\mathbf{R}_R = d\mathbf{e}_y$ are the position vectors of the two dots. As in Ref. 11, we have assumed that the center of the left dot is located at the origin of the coordinate system while the center of the right dot is placed on the y -axis with distance d , see Fig. 1 for a sketch. The two dots are assumed to have an equal radius of a and to be confined to the xy -plane in the underlying 2DEG. The coupling constants $\lambda_{\mathbf{q}}$ which depend on material parameters and on the wave vector \mathbf{q} will be specified below. To take into account a realistic dot geometry, we associate a form factor

$$F_{\xi}(\mathbf{q}) = \int d^3r n_{\xi}(\mathbf{r}) e^{-i\mathbf{q}\cdot\mathbf{r}} \quad (5)$$

to each dot, where $n_{\xi}(\mathbf{r})$ is the charge density distribution of the dot. In the following, the two dots are assumed to have identical form factors. With this the coupling Hamiltonian simplifies to^{11,17}

$$H_{SB} = \frac{\hbar}{2} \sigma_z \sum_{\mathbf{q}} g_{\mathbf{q}} (b_{\mathbf{q}}^{\dagger} + b_{-\mathbf{q}}), \quad (6)$$

with $g_{\mathbf{q}} = \lambda_{\mathbf{q}} F(\mathbf{q})(1 - e^{-i\mathbf{q}\cdot d\mathbf{e}_y})$. Notice that the phonons can propagate in all three dimensions and that the electron-phonon-coupling is not isotropic.¹¹ Having specified the coupling, we can now introduce the spectral density of the phonon bath which reads

$$J(\omega) = \sum_{\mathbf{q}} |g_{\mathbf{q}}|^2 \delta(\omega - \omega_{\mathbf{q}}). \quad (7)$$

As in Ref. 11, we specialize to linear acoustic phonons with velocity s ($s \approx 5 \times 10^3$ m/s for GaAs) and linear dispersion $\omega_{\mathbf{q}} = s|\mathbf{q}|$. Moreover, we only consider coupling to longitudinal piezoelectric phonons and neglect the contribution of the deformation potential which is justifiable at temperatures below 10 K for bulk GaAs material.^{11,18} This yields the coupling constant $|\lambda_{\mathbf{q}}|^2 = g_{\text{ph}}\pi^2 s^2 / (V|\mathbf{q}|)$, where g_{ph} is the dimensionless piezoelectric constant ($g_{\text{ph}} \approx 0.05$ for GaAs) and V being the volume of the unit cell. Assuming that the charge density distribution on the dot is Gaussian in the xy -plane and localized in the z -direction, one finds for the spectral density of the bath¹¹

$$J(\omega) = g_{\text{ph}}\omega \int_0^{\pi/2} d\theta \sin\theta e^{-\omega^2 a^2 \sin^2\theta/s^2} \times \left[1 - J_0\left(\frac{\omega d}{s} \sin\theta\right) \right]. \quad (8)$$

The spectral density is shown in the inset of Fig. 2 for the case of GaAs and a dot radius of $a = 60$ nm. The low-frequency behavior is superohmic, i.e., $J(\omega \rightarrow 0) \approx \alpha_{\text{SO}}\omega_c^{-2}\omega^3$ with $\alpha_{\text{SO}} = g_{\text{ph}}d^2/(6a^2)$, while the high-frequency tail falls off algebraically like $J(\omega \rightarrow \infty) \propto 1/\omega$. The crossover between these two limiting regimes occurs on a frequency scale $\omega_c = s/a \approx \tau_c^{-1}$. For GaAs and a typical dot radius of $a = 60$ nm, we obtain $\omega_c = 83$ GHz corresponding to an energy of $55 \mu\text{eV}$. As we will see below, the typical tunneling amplitudes Δ are comparable to this energy scale. This indicates that the Markov approximation could become problematic in this transition region. The cut-off frequency ω_c corresponds to the inverse of the time scale τ_c of the bath autocorrelation function which reads¹⁶

$$L(t) = L_R(t) + iL_I(t) = \frac{1}{\pi} \int_0^{\infty} d\omega J(\omega) \left[\coth \frac{\hbar\omega\beta}{2} \cos\omega t - i \sin\omega t \right] \quad (9)$$

The autocorrelation function $L(t)$ is shown in Fig. 2 for $T = 15$ mK for $a = 60$ nm and $d = 180$ nm.^{11,19} The algebraic decay at high frequencies determines the short time behavior of $L(t)$; notice the finite slope of $L_R(t)$ at $t = 0$, in contrast to zero slope of the usual exponential and Drude-shaped cut-off functions.¹⁶ The superohmic low frequency behavior of $J(\omega)$ yields a fast decay of $L(t)$ at long times. The often used Born-Markov approximation corresponds to replacing the strongly peaked real part $L_R(t)$ by a δ -function with the corresponding weight while the imaginary part $L_I(t)$ is often neglected. Moreover, we note that the dimensionless damping constant given by the prefactor α_{SO} of the low-frequency superohmic limit assumes the value $\alpha_{\text{SO}} = 0.075$ for the parameters quoted above. Thus, our results at small Δ can be

compared to those from a weak-coupling approach in terms of real-time path-integrals for the spin-boson model with a superohmic environment.¹⁶

III. THE QUASIADIABATIC PATH-INTEGRAL PROPAGATOR (QUAPI)

The dynamics of the qubit is characterized by the time evolution of the reduced density matrix $\rho(t)$ which is obtained after tracing out the bath degrees of freedom, i.e.,

$$\begin{aligned}\rho(t) &= \text{tr}_B U(t, 0) W(0) U^{-1}(t, 0), \\ U(t, 0) &= \mathcal{T} \exp \left\{ -\frac{i}{\hbar} \int_0^t dt' H \right\}.\end{aligned}\quad (10)$$

Here, $U(t, 0)$ denotes the propagator of the full system plus bath and \mathcal{T} denotes the time-ordering operator. $W(0)$ is the full density operator at initial time set at $t = 0$. We assume standard factorizing initial conditions,¹⁶ i.e., $W(0) \propto \rho(0) \exp[-H_B/(k_B T)]$, where the bath is at thermal equilibrium at temperature T and the system is prepared according to $\rho(0)$. Throughout this work, we always start from the qubit state $\rho(0) = |L\rangle\langle L|$.

The technique which we use to calculate $\rho(t)$ is the well established iterative tensor multiplication algorithm derived for the quasiadiabatic propagator path integral (QUAPI).¹³ It is a numerically exact algorithm, as also, for instance, the real-time quantum Monte Carlo method is.²⁰ It has been successfully tested and adopted in various problems of open quantum systems, with and without external driving.^{13,14,15} For details of this algorithm, we refer to previous work^{13,14,15} and here only address the ingredients which are important to our calculations.

The algorithm relies on the symmetric Trotter splitting of the short-time propagator $U(t_{k+1}, t_k)$ into system (H_S) and bath (H_B) parts on a time slice of length Δt . The bath dynamics can be solved exactly yielding a Feynman-Vernon-type influence functional¹⁶ while the system is propagated exactly by solving the Schrödinger equation. The neglect of higher order terms of the full propagator causes an error of the order of Δt^3 . The Trotter splitting allows to calculate an approximate value of the true result for the observable of interest, with an error depending on Δt . As shown in Ref. 21, this error vanishes proportional to Δt^2 as $\Delta t \rightarrow 0$. Thus, by extrapolation of the results for $\Delta t \rightarrow 0$, the Trotter error can be eliminated completely (the details of this procedure will be discussed elsewhere²²).

The interaction of the system with the bath induces internal transitions in both and creates intercorrelations between them (memory); the latter are described by the autocorrelation function $L(t)$ given in Eq. (9). For the phonon bath, these correlations decay on a time scale given by the correlation time τ_c . This motivates us to neglect such long-time correlations beyond a memory time τ_{mem} and to break up the influence kernels into pieces of total length $\tau_{\text{mem}} = K \Delta t$, where K denotes the number of time steps over which the memory is fully taken into account.

The two strategies mentioned above are countercurrent: For the Trotter splitting, a small time step Δt is desirable, thus decreasing τ_{mem} for a fixed K . On the other hand, a large τ_{mem} is wanted in order to take a long memory range into account. Nevertheless, converged results can be obtained in the following way: (i) We choose τ_{mem} such that we include all the relevant parts of the correlation function $L(t)$. Quantitatively, this can be done by requiring $L_R(\tau_{\text{mem}})/L_R(0) \leq 10^{-3}$ in the asymptotic regime. (ii) We choose K such that the resulting $\Delta t = \tau_{\text{mem}}/K$ is small enough to ensure that we are in the regime which allows extrapolation for $\Delta t \rightarrow 0$ (see above). This procedure allows to completely eliminate the Trotter error. We note that the choice of K is limited to a maximum of $K = 12$ for reasonable numerical practicability on a personal computer.

IV. THE Q -FACTOR OF COHERENT CHARGE OSCILLATIONS

We have adjusted the QUAPI algorithm to the phonon spectral density (8) and determine the charge population $\rho_{11}(t)$ of the left dot as a function of time for the initial condition $\rho_{11}(0) = 1$. A typical example of the resulting damped oscillatory behavior is shown in Fig. 3 where the exact QUAPI results are depicted by the symbols (\blacklozenge) for the case $\Delta = 27\mu\text{eV}$, $T = 15\text{ mK}$ and $K = 12$. To extract the damping rate γ and the oscillation frequency Ω , we fit an exponentially decaying cosine to the numerical data. The result of the fit is also shown in Fig. 3 as solid line. The fit yields $\Omega_{\text{QUAPI}} = 0.98\omega_c$ for the oscillation frequency and $\gamma_{\text{QUAPI}} = 5.27 \times 10^{-3}\omega_c$ for the decay constant.

The ratio of γ and Ω fixes the quality factor according to the convention $Q = \Omega/(\pi\gamma)$. Evaluating Q allows us to investigate the dependence of the coherence of the charge oscillations on various experimental parameters. Figure 4 shows the Q -factor as a function of the tunneling amplitude Δ obtained with the numerically exact QUAPI algorithm (+). For illustration, we have used parameters from the experimental setup of Ref. 19. Since our model contains realistic assumptions about the geometry of the DQD and the materials characteristics, the predictions of the QUAPI calculations in this case can be considered quite accurate. Two regimes exist: (i) At small Δ , Q decreases with increasing Δ (see below) while (ii) at large Δ , Q increases again with increasing Δ . The crossover in between occurs when the energy splitting between the qubit states coincides with the maximum of the spectral density $J(\omega)$, i.e., when $2\Delta = \omega_c$. Then, the damping is most efficient and thus the rate γ is maximal. Notice that realistic values for the tunneling amplitudes Δ fall in the range of the bath correlation frequency scale ω_c (see upper axis of Fig. 4, where Δ is scaled with respect to ω_c).

Since the coupling to the phonons is rather weak (cf. the value of $\alpha_{\text{SO}} = 0.075$ for the superohmic coupling constant at low frequencies), it is tempting to compare our exact results to simple, approximate analytical results obtained from real-time path-integral formalism in the regime of weak-coupling.¹⁶ However, we remark that one needs to have in mind that the

algebraic decay of the spectral density at large frequencies is by itself not taken into account while deriving the approximate result. Thus, only the superohmic low-frequency part can be expected to yield a reasonable agreement. The weak-coupling results are given by¹⁶

$$\Omega = 2\Delta[1 - 2 \operatorname{Re} u(2i\Delta)]^{1/2} \quad (11)$$

and

$$\gamma = \frac{1}{4} J(2\Delta) \coth \frac{\hbar\Delta}{k_B T}, \quad (12)$$

where

$$u(z) = \frac{1}{2} \int_0^\infty d\omega \frac{J(\omega)}{\omega^2 + z^2} \left(\coth \frac{\hbar\omega}{2k_B T} - 1 \right). \quad (13)$$

With this, we can compute the time evolution of charge population of the left dot in the weak-coupling approximation which is shown in Fig. 3 (dashed line) for the same parameters as above. The deviation from the exact result for the chosen parameters due to non-Markovian effects is striking and also illustrated by the numerical values $\Omega = 3.0\omega_c$ and $\gamma = 5.6 \times 10^{-3}\omega_c$.

The resulting Q -factor is shown in Fig. 4 (solid line, “wca”). Since the results in Eqs. (11) and (12) are obtained by linearization with respect to the damping constant g_{ph} , they are equivalent to a Born-Markovian approximation. We find noticeable deviations for intermediate and large values of Δ . From Eq. (11) it follows that the oscillation frequency Ω is renormalized by the term involving $u(2i\Delta)$ stemming from one-phonon interblip correlations in the self-energy.¹⁶ We find that at small Δ these corrections are negligible, while they increasingly become important at larger Δ , pointing to a non-Markovian dynamics in this regime. Note that the qualitative behavior of Q versus Δ is similar to that found in Ref. 11 within the Born-Markovian master equation approach. However, the absolute numbers disagree.

To understand the results at small tunneling amplitudes, we zoom into the small- Δ region and show the QUAPI results in Fig. 5 (+, right ordinate scale) together with the results from the weak-coupling approximation (solid line) obtained from Eqs. (11) and (12). Therefore, we have used the pure superohmic spectral density with an exponential cutoff with frequency $\Omega_c \gg \Delta$, i.e., $J(\omega) = \alpha_{\text{SO}} \omega_c^{-2} \omega^3 \exp(-\omega/\Omega_c)$ with $\alpha_{\text{SO}} = 0.075$ and $\Omega_c = 10\omega_c$. We find a good agreement between both results in the limit of small Δ , thus justifying that the dynamics at small Δ is Markovian. Nevertheless, note that even in this frequency range deviations between the exact and the approximate solution do appear. As a further check, we also compare the results of both the numerically exact and the analytical approach for Q for a pure Ohmic environmental spectral density $J(\omega) = \alpha\omega \exp(-\omega/\omega_c)$ for $\alpha = 0.05$. Both the QUAPI (▼) and the approximative weak-coupling solution (dashed line) coincide. The Q -factor decreases monotonically for decreasing Δ since the Ohmic low-frequency modes are not suppressed strongly enough in comparison with the superohmic case. Although the dynamics is Markovian for small

Δ , non-Markovian corrections appear to be relevant at intermediate values of Δ . Because realistic values for the tunneling splitting Δ are also of the order of ω_c , the role of the large frequency tail $\propto 1/\omega$ still is not negligible and cannot be appropriately taken into account within a Born-Markovian master equation.

The sensitivity of the Q -factor on the lattice temperature T of the GaAs host is shown in Fig. 6 for a small and a large tunneling amplitude Δ . Note that for the latter the corresponding Born-Markov results have been shown not to be reliable due to noticeable non-Markovian corrections which can be observed in our data. Another parameter which is adjustable in the DQD design is the dot radius a . The dependence of Q on a is depicted in Fig. 7 for a large and a small tunneling amplitude for a fixed ratio $d/a = 3$. We find that Q decreases monotonically with increasing a for small value of Δ , while it increases with increasing a for large value of Δ , qualitatively similar to the findings in Ref. 11. Note, however, the sizeable differences in the absolute numbers which are due to the non-Markovian corrections.

Finally, we address the recent experiment of Hayashi *et al.*⁷ These authors implemented a GaAs DQD in the bias-pulsing mode. During the pulse, the tunneling amplitude is constant. The bias pulse is ramped up on a time scale of 100 ps. The tunneling amplitude has been estimated as $\Delta = 5 \mu\text{eV}$. The lattice temperature was $T = 20$ mK, while the effective dot radius and the interdot distance have been estimated to be $a \approx 50$ nm and $d \approx 225$ nm, respectively. For this combination of parameters, the QUAPI method yields $Q = 352$ which has to be compared with the experimental value of $Q = 3$. On the other hand, the weak-coupling solution of Eqs. (11) and (12) yields $Q = 539$. Two important conclusions can be drawn from these numbers. First, the Born-Markov approximation underestimates decoherence in these systems and non-Markovian corrections are quite noticeable. Second, our exact result differs from the experimental value by a factor of roughly 100, indicating that the role of the phonons for the decoherence is indeed of minor importance to understand the reported experimental results. Other sources of decoherence like voltage fluctuations from the electromagnetic environment or background charge fluctuations exist and have to be taken into account for an accurate description for so far realized charge-based DQD qubits.

However, our result go beyond this point: Our predicted exact values of the Q -factors represent a fundamental upper limit on the possibility to improve coherence of DQD charge qubits since phonon decoherence represents an intrinsic decoherence mechanism which can hardly be overcome. This has to be noticed also in view of the DiVincenzo criteria²³ for a possible realization of a quantum computer.

V. CONCLUSIONS

To summarize, we have obtained numerically exact results for the Q -factor of the decaying charge oscillations in a double quantum dot upon using the real-time quasiadiabatic propagator path integral (QUAPI). Realistic assumptions on the form

of the environmental phonon spectral density entered in our model via geometrical form factors and materials characteristics. No fitting parameters of any sort were utilized. We have investigated the quality (Q -) factor as a function of the tunneling splitting and have compared our results with those obtained from a weak-coupling approximation within an analytical approach in terms of real-time path-integrals. We find that the regime of small tunneling amplitudes is appropriately covered by the Markovian description. However, at larger (but still realistic) values of the tunneling amplitude, non-Markovian corrections appear and are relevant. Moreover, we have determined the temperature dependence of Q -factor as well as its dependence on the dot radius. From a comparison with the result obtained in an experimental realization of a double quantum dot charge qubit, we find that the theory predicts a Q -factor two orders of magnitude larger than the measured value. This leads to the conclusion that phonon decoherence is a subordinate mechanism in GaAs quantum dots realized with present state-of-the-art technology. Clearly, other forms of coupling to the external environment prevail for those already realized devices. However, our results also represent a fundamental upper limit to the coherence of DQD

charge qubits which can hardly be overcome due to its intrinsic nature.

It would be interesting to extend the QUAPI calculation to Si-based charge qubits, which have recently been implemented.⁹ Since Si has inversion symmetry, piezoelectric phonons do not occur and one needs to include deformation potential phonons in the calculations. The decoherence induced by the electron-phonon coupling is likely to be smaller than in GaAs. However, for the deformation potential case, $\lambda_q \sim \sqrt{|q|}$. Thus, if on one hand we expect a strong superohmic behavior at low frequencies, on the other hand, a very slow decay of the spectral function at high frequencies should occur. That may provide an even stronger non-Markovian dynamics and have implications for other implementations, such as Si:P donor-based charge qubits.^{24,25,26}

Acknowledgments

We thank Harold Baranger, Stephan Weiss, Reinhold Egger and Frank Wilhelm for discussions.

-
- ¹ W. G. van der Wiel, S. De Franceschi, J. M. Elzerman, T. Fujisawa, S. Tarucha, and L. P. Kouwenhoven, *Rev. Mod. Phys.* **75**, 1 (2003).
- ² T. Brandes, *Phys. Rep.* **408**, 315 (2005).
- ³ R. H. Blick and H. Lorenz, in *Proceedings of the IEEE International Symposium on Circuits and Systems*, Geneva, Switzerland, 2000, edited by J. Calder (IEEE, Piscataway, NJ, 2000), Vol. II, p. 245.
- ⁴ T. Tanamoto, *Phys. Rev. A* **61**, 022305 (2000).
- ⁵ L. Fedichkin and A. Fedorov, *Phys. Rev. A* **69**, 032311 (2004); L. Fedichkin, M. Yanchenko, and K. A. Valiev, *Nanotechnology* **11**, 387 (2000).
- ⁶ T. Brandes and T. Vorrath, *Phys. Rev. B* **66**, 075341 (2002).
- ⁷ T. Hayashi, T. Fujisawa, H. D. Cheong, Y. H. Jeong, and Y. Hiraizumi, *Phys. Rev. Lett.* **91**, 226804 (2003).
- ⁸ J. R. Petta, A. C. Johnson, C. M. Marcus, M. P. Hanson, and A. C. Gossard, *Phys. Rev. Lett.* **93**, 186802 (2004).
- ⁹ Coherent quantum oscillations of charge in Si-based *isolated* double quantum dots have recently been observed in J. Gorman, D. G. Hasko, and D. A. Williams, *Phys. Rev. Lett.* **95**, 090502 (2005).
- ¹⁰ M. Thorwart and P. Hänggi, *Phys. Rev. A* **65**, 012309 (2002).
- ¹¹ S. Vorojtsov, E. R. Mucciolo, and H. U. Baranger, *Phys. Rev. B* **71**, 205322 (2005).
- ¹² V. N. Stavrou and X. Hu, *Phys. Rev. B* **72**, 075362 (2005).
- ¹³ D. E. Makarov and N. Makri, *Chem. Phys. Lett.* **221**, 482 (1994); N. Makri and D. E. Makarov, *J. Chem. Phys.* **102**, 4600 (1995); 4611 (1995); N. Makri, *J. Math. Phys.* **36**, 2430 (1995).
- ¹⁴ M. Thorwart, P. Reimann, P. Jung, and R. F. Fox, *Chem. Phys.* **235**, 61 (1998).
- ¹⁵ M. Thorwart, P. Reimann, and P. Hänggi, *Phys. Rev. E* **62**, 5808 (2000).
- ¹⁶ U. Weiss, *Quantum Dissipative Systems* (World Scientific, Singapore, 1999).
- ¹⁷ T. Brandes and B. Kramer, *Phys. Rev. Lett.* **83**, 3021 (1999).
- ¹⁸ As shown in Ref. 12, deformation potential phonons are only important for ultra small DQD setups. Optical phonons are too high in energy (~ 36 meV) and can be safely neglected.
- ¹⁹ H. Jeong, A. M. Chang, and M. R. Melloch, *Science* **293**, 2221 (2001).
- ²⁰ R. Egger and C. H. Mak, *Phys. Rev. B* **50**, 15210 (1994).
- ²¹ R. M. Fye, *Phys. Rev. B* **33**, 6271 (1986).
- ²² J. Eckel, S. Weiss, and M. Thorwart, in preparation.
- ²³ D. P. DiVincenzo, *Fortschr. Phys.* **48**, 771 (2000).
- ²⁴ S. D. Barrett and G. J. Milburn, *Phys. Rev. B* **68**, 155307 (2003).
- ²⁵ L. C. L. Hollenberg, A. S. Dzurak, C. Wellard, A. R. Hamilton, D. J. Reilly, G. J. Milburn, and R. G. Clark, *Phys. Rev. B* **69**, 113301 (2004).
- ²⁶ X. Hu, B. Koiller, and S. Das Sarma, *Phys. Rev. B* **71**, 235332 (2005).

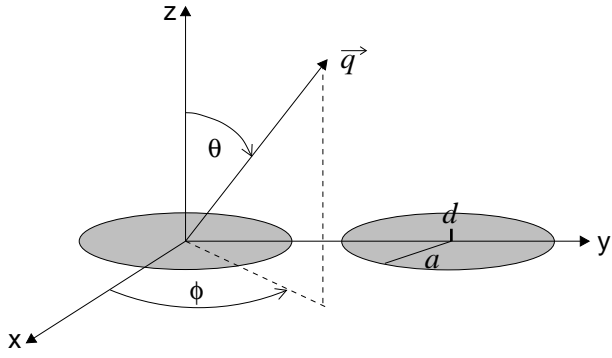


FIG. 1: Sketch of the geometry of the double quantum dot charge qubit and the various angles of the phonon propagation.

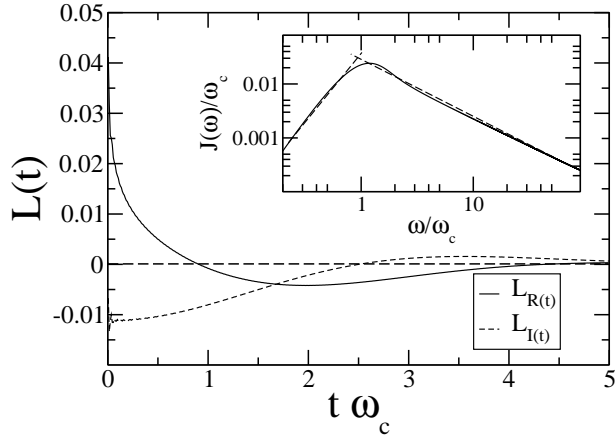


FIG. 2: The bath autocorrelation function (response function) $L(t) = L_R(t) + iL_I(t)$ for the spectral density $J(\omega)$ (inset) of the phonon bath for the case of GaAs with $g_{\text{ph}} = 0.05$, $s = 5 \times 10^3$ m/s, a dot radius of $a = 60$ nm, and interdot distance $d = 180$ nm. Temperature is $T = 15$ mK. The dashed lines in the inset mark the superohmic limit $J(\omega \rightarrow 0) = \alpha_{\text{SO}} \omega_c^{-2} \omega^3$ at low frequencies and the high-frequency limit $J(\omega \rightarrow \infty) \propto 1/\omega$.

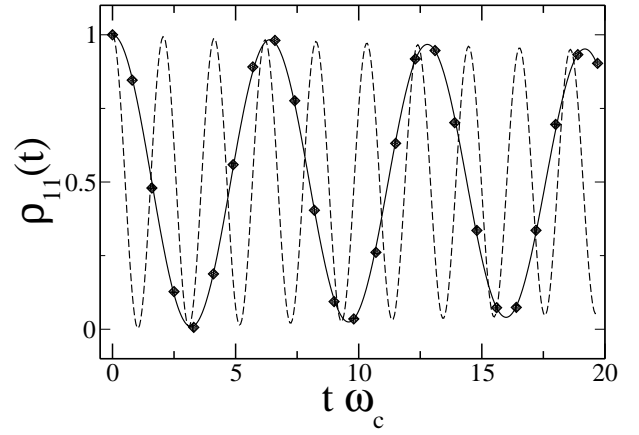


FIG. 3: Time evolution of the charge population of the left dot for the case $\Delta = 27 \mu\text{eV}$ and $T = 15$ mK. Shown are the exact results obtained from QUAPI (\blacklozenge) and the result of a fit of an exponentially decaying cosine to $\rho_{11}(t)$ (solid line). The dashed line indicates the result of a weak-coupling (Born-Markov) approximation using Eqs. (11) and (12) for the same parameters. Deviations from the exact results are striking. The remaining parameters are the same as in Fig. 2.

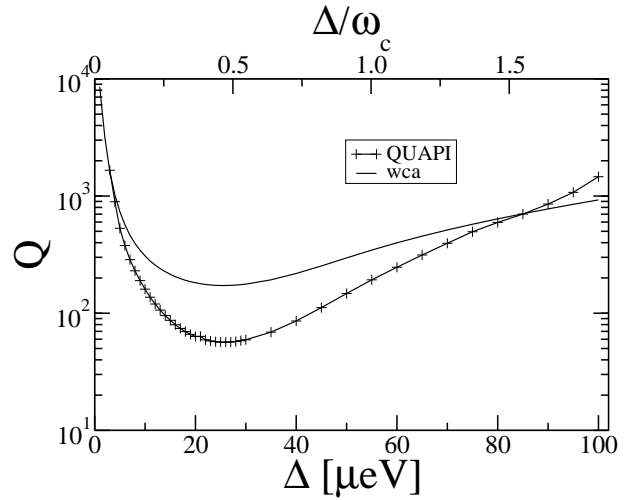


FIG. 4: The quality factor Q of the coherent charge oscillations as a function of the tunneling amplitude Δ in natural units (lower scale) and scaled with respect to ω_c (upper scale). The data shown are obtained with QUAPI (+) using the phonon spectral density (Eq. (8)) and with the weak-coupling approximation (wca) of Eqs. (11) and (12). The parameters are the same as in Fig. 2.

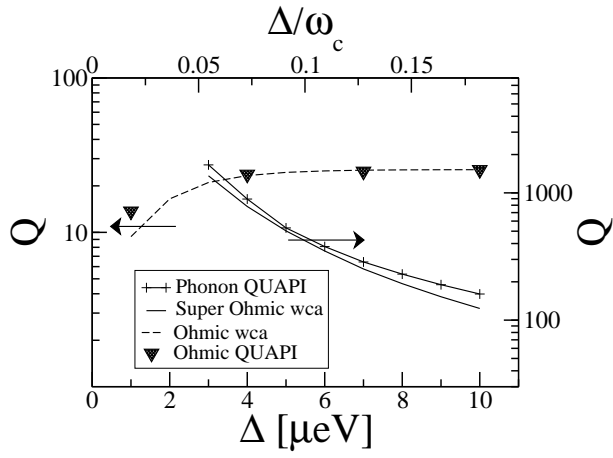


FIG. 5: Zoom into the small- Δ region. Shown are the QUAPI results for the phonon (+) and the pure Ohmic (\blacktriangledown) spectral density. In addition, they are compared with the approximate analytical, weak-coupling results of Eqs. (11) and (12) for the superohmic (solid line) and the ohmic (dashed line) cases. The parameters are: (i) Ohmic case, $\alpha = 0.05$ and (ii); superohmic case, $\alpha_{SO} = 0.075$. For all cases, $T = 15$ mK.

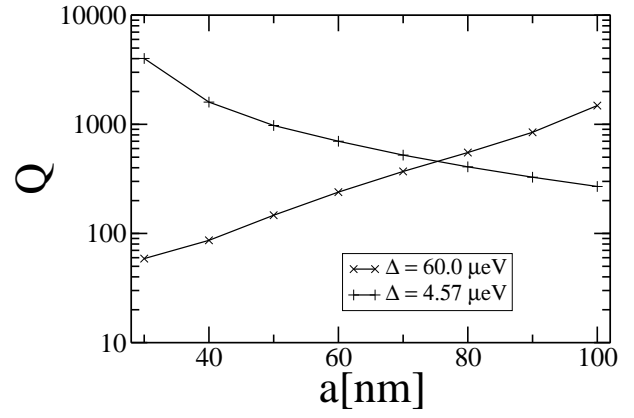


FIG. 7: Q -factor as a function of the dot radius a for two different tunneling amplitudes Δ and for a fixed ratio $d/a = 3$. The remaining parameters are the same as in Fig. 2.

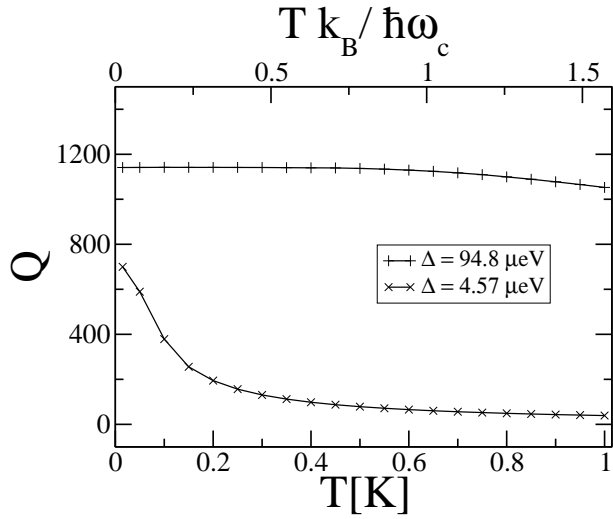


FIG. 6: Q -factor as a function of temperature for two different tunneling amplitudes Δ . The remaining parameters are the same as in Fig. 2.